The Company of **Biologists**

RESEARCH ARTICLE

How the bending kinematics of swimming lampreys build negative pressure fields for suction thrust

Brad J. Gemmell[1,2], Stephanie M. Fogerson[2], John H. Costello[2,3], Jennifer R. Morgan[2], John O. Dabiri[4] and Sean P. Colin[2,5,*]

ABSTRACT

Swimming animals commonly bend their bodies to generate thrust. For undulating animals such as eels and lampreys, their bodies bend in the form of waves that travel from head to tail. These kinematics accelerate the flow of adjacent fluids, which alters the pressure field in a manner that generates thrust. We used a comparative approach to evaluate the cause-and-effect relationships in this process by quantifying the hydrodynamic effects of body kinematics at the body–fluid interface of the lamprey, *Petromyzon marinus*, during steady-state swimming. We compared the kinematics and hydrodynamics of healthy control lampreys to lampreys whose spinal cord had been transected mid-body, resulting in passive kinematics along the posterior half of their body. Using high-speed particle image velocimetry (PIV) and a method for quantifying pressure fields, we detail how the active bending kinematics of the control lampreys were crucial for setting up strong negative pressure fields (relative to ambient fields) that generated high-thrust regions at the bends as they traveled all along the body. The passive kinematics of the transected lamprey were only able to generate significant thrust at the tail, relying on positive pressure fields. These different pressure and thrust scenarios are due to differences in how active versus passive body waves generated and controlled vorticity. This demonstrates why it is more effective for undulating lampreys to pull, rather than push, themselves through the fluid.

KEY WORDS: Hydrodynamics, Biomechanics, Propulsion, Fish, Vortex, Flexible bending

INTRODUCTION

Aquatic animals significantly outperform man-made aquatic vehicles because they are able to move in water with greater efficiency and maneuverability (Bandyopadhyay, 2005; Gemmell et al., 2013). Animals achieve these performance attributes by effectively transferring the momentum of body movements to the surrounding fluid in a manner that efficiently produces and controls thrust production. Understanding the mechanics of how this is achieved is fundamental to understanding how animals swim.

For most animals greater than a couple of millimeters in length, the momentum and energy they transfer to the surrounding fluid are

[1]Department of Integrative Biology, University of South Florida, Tampa, FL 33620, USA. [2]The Eugene Bell Center for Regenerative Biology and Tissue Engineering, Marine Biological Laboratory, Woods Hole, MA 02543, USA. [3]Biology Department, Providence College, Providence, RI 02918, USA. [4]Departments of Civil & Environmental Engineering and Mechanical Engineering, School of Engineering, Stanford University, Stanford, CA 94305, USA. [5]Marine Biology and Environmental Science, Roger Williams University, Bristol, RI 02809, USA.

*Author for correspondence (scolin@rwu.edu)

S.P.C., 0000-0003-4463-5588

packaged in the form of vortices (Dickinson et al., 2000). This convenient nature of water has enabled scientists to quantify the amount of circulation in the fluid to estimate the amount of thrust generated by swimming animals (termed the impulse of the fluid) and their hydrodynamic efficiency (Bartol et al., 2009; Batchelor, 1973; Dabiri et al., 2010; Krueger and Gharib, 2003; Linden and Turner, 2004). Quantification of wake properties behind swimming animals, such as impulse, has contributed greatly to our understanding of propulsion (Nauen and Lauder, 2002; Tytell, 2004). However, much less is understood about how animal body kinematics generate and control vortices at the body–fluid interface and how these fluid structures relate to thrust production. Quantification of relationships at this mechanistic level of propulsion is required to understand how animal form and kinematics control thrust.

The morphology and kinematics of animal propulsors are characteristically similar in that they are almost universally flexible. In fact, the kinematics of how propulsors bend while moving to generate thrust are remarkably similar among most animals that swim or fly (Bale et al., 2015; Lucas et al., 2014). This suggests that the role that bending kinematics play in generating thrust is similar among swimming and flying animals. Studies have shown that the magnitude of bending of flexible propulsors affects the amount of thrust produced and that thrust increases with increasing flexibility of propulsors up to an optimal level, after which increasing flexibility diminishes thrust (Alben, 2008; Colin et al., 2012; Lucas et al., 2015; Mountcastle and Daniel, 2010; Tytell et al., 2010). However, we have much less of an understanding of the mechanisms through which bending kinematics interact with adjacent fluids to enhance thrust. One effect of bending is that it enhances negative pressure regions of the fluid adjacent to the inflexion point of the bending appendage (Colin et al., 2012; Li et al., 2012; Nakata and Liu, 2012). This serves to accelerate more fluid than fluid around rigid propulsors, which enhances the momentum of the surrounding fluid. We previously demonstrated that lampreys generate negative pressure regions along their undulating body that serve as the primary sources of thrust production during steady-state swimming (Gemmell et al., 2015). However, we did not address how the bending kinematics interact with the surrounding fluid to generate negative pressure regions that can contribute to thrust. Much more needs to be known about how the bending of propulsors interacts with adjacent fluid in order to understand how flexibility influences how animals generate and control thrust production.

Anguilliform swimmers, which include lampreys, are a subset of swimmers that use their flexible bodies for propulsion. A broad range of animal taxa, ranging from invertebrate leeches (Chen et al., 2011) to vertebrate fishes (Tytell and Lauder, 2004) and reptiles (Graham et al., 1987), swim using similar anguilliform body kinematics. All of these swimmers actuate muscles to generate a

bending wave that travels the length of most of their body (e.g. Williams et al., 1989). It has been well-documented that the traveling wave generates vortices (which have been termed proto-vortices when attached to the swimming body) that move down along the body with the wave (Chen et al., 2011; Müller et al., 1997; Muller et al., 2001). For some species, this process produces thrust along most of the body, whereas, for other species, such as eels, thrust is primarily produced at the posterior end (Lauder and Tytell, 2005; Tytell and Lauder, 2004). Very little is understood about how these disparate kinematics each generate and control vorticity fields along the body in order to control thrust production. Furthermore, it is not understood how less-than-optimal kinematics alter vortex generation and control.

Our goal was to quantify how bending kinematics are related to the generation and control of vortices, and how these hydrodynamic features relate to pressure fields and thrust along the body of lampreys with normal and non-normal swimming kinematics. The properties of anguilliform kinematics and how they affect vorticity have been previously well quantified (Lauder and Tytell, 2005; Müller et al., 1997; Tytell and Lauder, 2004); however, the role that the different kinematic and hydrodynamic properties play in determining pressure fields and thrust is not known. To experimentally evaluate this, we compared the kinematics and hydrodynamics of healthy sea lampreys (*Petromyzon marinus*) to those whose spinal cord was transected at a mid-body position. This enabled us to compare the role of both kinematics and the importance of active (versus passive) control of kinematics in determining propulsion.

MATERIALS AND METHODS
Animals and dissection protocol
The sea lampreys (*Petromyzon marinus*, Linnaeus 1758) used in this study were late-stage larvae (9–12 cm; ∼5–7 years old). They were acquired from Lamprey Services (Ludington, MI) and were maintained at room temperature (23–25°C) in 10-gallon aquaria. Prior to surgery, lampreys were anesthetized with Finquel MS-222 (0.1 g l^{-1} tank water; Argent Chemical Laboratories). Spinal cord transections were performed as detailed previously (Jacobs et al., 1997; Oliphint et al., 2010). Briefly, each lamprey was placed in a Sylgard-lined Petri dish on a paper towel moistened in oxygenated lamprey Ringers (100 NaCl, 2.1 KCl, 2.6 CaCl$_2$, 1.8 MgCl$_2$, 4 glucose, 0.5 glutamine, 2 HEPES, pH 7.4). A dorsal incision was made approximately halfway down the length of the body, just above the dorsal fin, through the skin, musculature and fat tissue in order to expose the spinal cord. Then, the spinal cord was completely transected at the mid-body with a single horizontal cut made with fine iridectomy scissors. The incision was closed with a single suture (Ethilon 6-0 black monofilament nylon; Johnson & Johnson, Langhorn, PA). At the mid-body, larval lampreys are typically ∼5 mm wide. Typically, the dorsal incision during this surgery is estimated to be ∼3–4 mm, and it is easily closed with a single suture, resulting in complete wound healing. A similar procedure was performed on the control lampreys, except that the incision was made more rostrally, in the gill region, and the spinal cord was not transected. This controlled for effects of the operation on lamprey behavior. Both control and spinal-transected lampreys were capable of swimming immediately after they recovered from anesthesia (half an hour to an hour) because the rostral spinal circuits that initiate swimming were still intact. We allowed the lampreys to recover for 2 weeks in a holding tank before swimming experiments were performed. By 2 weeks, the incision has healed and spinal neurons start to re-grow (Zhang et al., 2005). Body

kinematic analyses were also performed on the mid-body-transected individuals before their operation (Fig. 1G, white triangles). This analysis shows that, before surgery, their kinematics were very similar to the control lampreys. All procedures were approved by the Institutional Animal Care and Use Committee at the Marine Biological Laboratory and in accordance with standards set by the National Institutes of Health (NIH).

Experimental setup and video processing
To quantify swimming kinematics and hydrodynamics, lampreys were video recorded in a 1.5×0.5 m acrylic aquarium filled with 5 cm of oxygenated lamprey tank water. Swimming animals were videoed at 1000 fps through the bottom of the aquarium using a Photron Fastcam 1024 PCI video camera. Two-dimensional particle image velocimetry (PIV) analysis was used to quantify the fluid motions around the lamprey. PIV was done by seeding the water with 10 µm hollow glass beads (LaVision, Inc.). The field of view
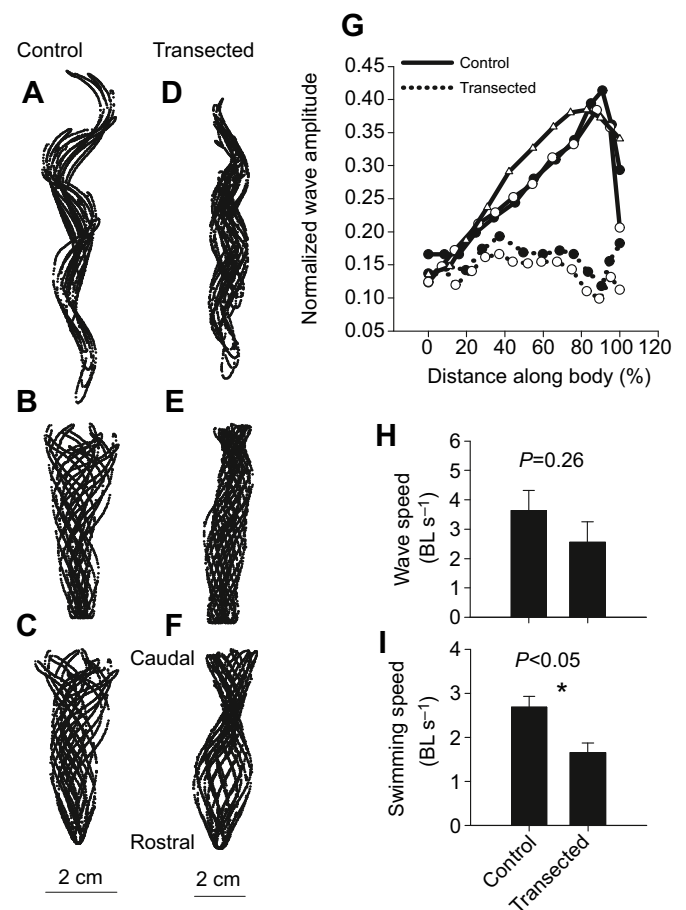

Fig. 1. Kinematics of control and mid-body-transected lampreys. Outlines are of free-swimming kinematics (A,D), kinematics with head held constant in the vertical direction (B,E) and kinematics with head held constant in both the horizontal and vertical directions (C,F). In all outlines the head (rostral) is at the bottom and tail (caudal) at the top. (G) Comparison of the wave amplitude (normalized by body length) shows that the amplitude of the wave generated by the control lampreys increases steadily to the tail, whereas the wave amplitude from transected fish remains relatively constant (each line is a different individual). (H) Means±s.d. wave speeds showing that they did not differ (Student's *t*-test, *N*=3 control and 2 mid-body transected). (I) Means±s.d. swimming velocity showing that the control lamprey swam significantly faster than the mid-body-transected lamprey (Student's *t*-test, *N*=3 control and 2 mid-body transected). BL, body length.
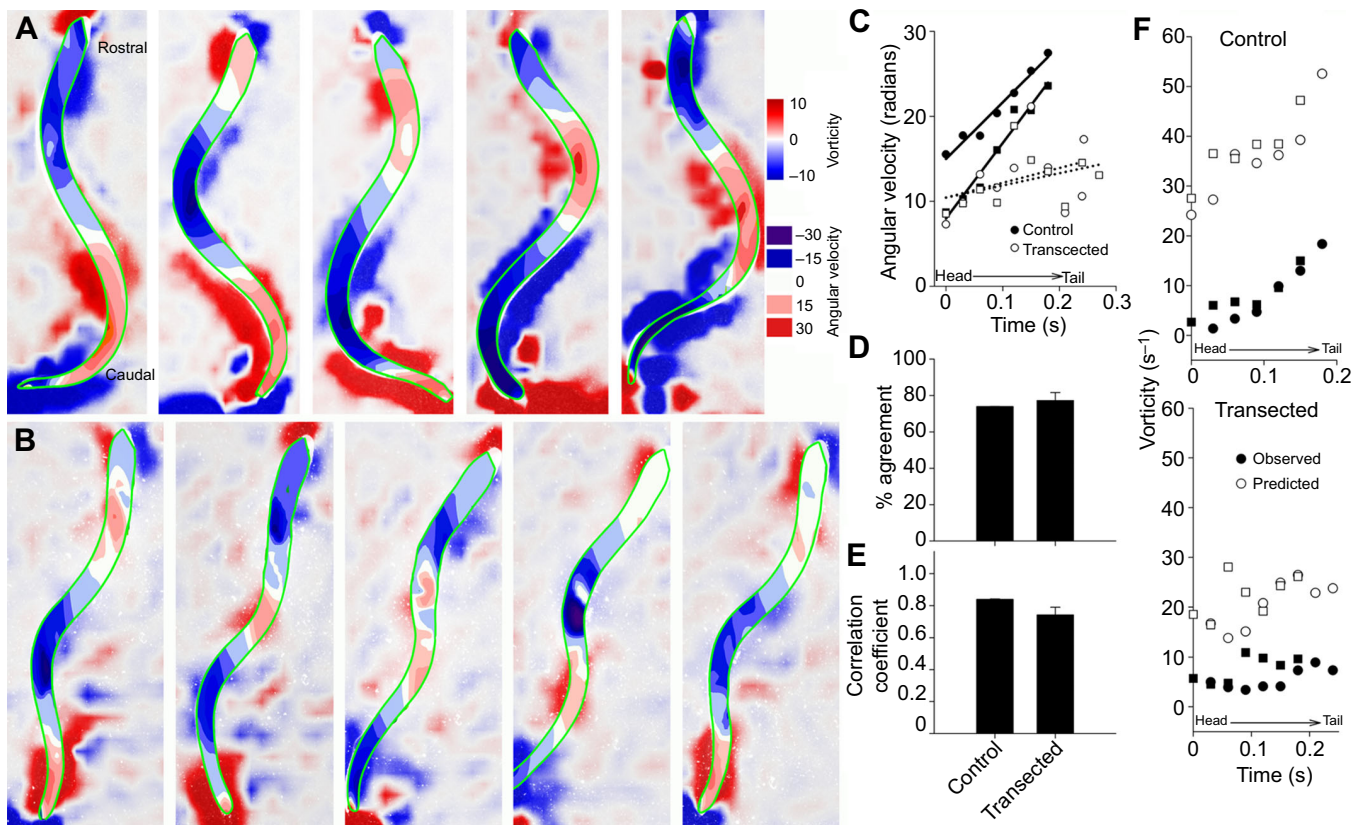
Fig. 2. Body surface rotation and fluid vorticity. (A,B) Body surface rotation [measured as angular velocity (ω)] of (A) control and (B) mid-body-transected lampreys over time (0.02 s interval; contours inside the body outline are based on surface body rotation, whereas contours outside are fluid vorticity measured from particle image velocimetry). (C) The angular velocity of the control lampreys increased steadily from head to tail (mean r^2=0.97±0.01), whereas that of the transected lampreys did not (mean r^2=0.15±0.02; circle and squares are different control and transected individuals). (D) Means±s.d. percent agreement of the direction of the body surface rotation and the direction of the fluid vorticity, and (E) means±s.d. correlation coefficient of magnitude of rotation and vorticity. (F) Maximum observed vorticity of the vortex and the vorticity predicted by the body rotation (where vorticity=2×ω).

was illuminated with a light sheet that was oriented horizontally and directed perpendicular to the camera angle, and was generated using two lasers (532 nm, 600 mW continuous wave) placed on opposite sides of the aquarium. Using two lasers eliminated shaded regions around the swimming lampreys and enabled us to thoroughly quantify the flow around the animals. The laser light did not seem to affect the lampreys' swimming behaviors. Lampreys started swimming at one end of the aquarium and the camera was positioned at the opposite end so that, by the time the lamprey reached the field of view, they were swimming in steady state without any acceleration. The only video sequences used were those where the velocity averaged over the entire sequence remained constant. However, whereas the average velocities remained constant, the instantaneous velocities at any moment during each swim cycle were continuously changing (see Fig. S1). The velocity vectors of particles illuminated in the laser sheet were quantified from sequential images that were analyzed using a cross-correlation algorithm (DaVis 7.2, LaVision Software).

Kinematic and hydrodynamic analysis

Image pairs (time delay=3000 μs) were analyzed with shifting overlapping interrogation windows of decreasing size (64×64 pixels, then 16×16 pixels). Digital masking of the body of the fish prior to image interrogation confirmed the absence of surface artifacts in the PIV measurements. Velocity and vorticity field data were exported from DaVis and later used to calculate various fluid

quantities using an in-house MATLAB code (MathWorks, Inc.). Circulation was quantified as:

$$\Gamma(t) = \int \omega(x, y, t) \, dxdy, \qquad (1)$$

where ω is a single value of vorticity at a location (x, y) and time (t) within the vorticity field. Boundaries of the vorticity region used for circulation measurements were defined by a minimum vorticity of $2 \, s^{-1}$. The lower vorticity boundary was selected because it was 10% of peak vorticity and was a robust boundary that was reliably identifiable. Patterns of how circulation changed along the body were not sensitive to different lower vorticity boundaries.

Swimming kinematics were quantified by hand using ImageJ (NIH) software and an in-house MATLAB program. Raw images of the freely swimming animals were input to a custom program in MATLAB that automatically identified the boundary of the animal body based on image contrast at the solid–fluid interface between the animal body and the surrounding fluid. Sixty equally spaced control points along the interface were used to define the animal body shape in each frame. The local body surface rotation was computed by first measuring the angle of the line segment connecting adjacent control points, and then computing the rate of change of that angle in a lab-fixed frame. The body surface vorticity was determined based on the value of vorticity in the fluid nearest to each control point.
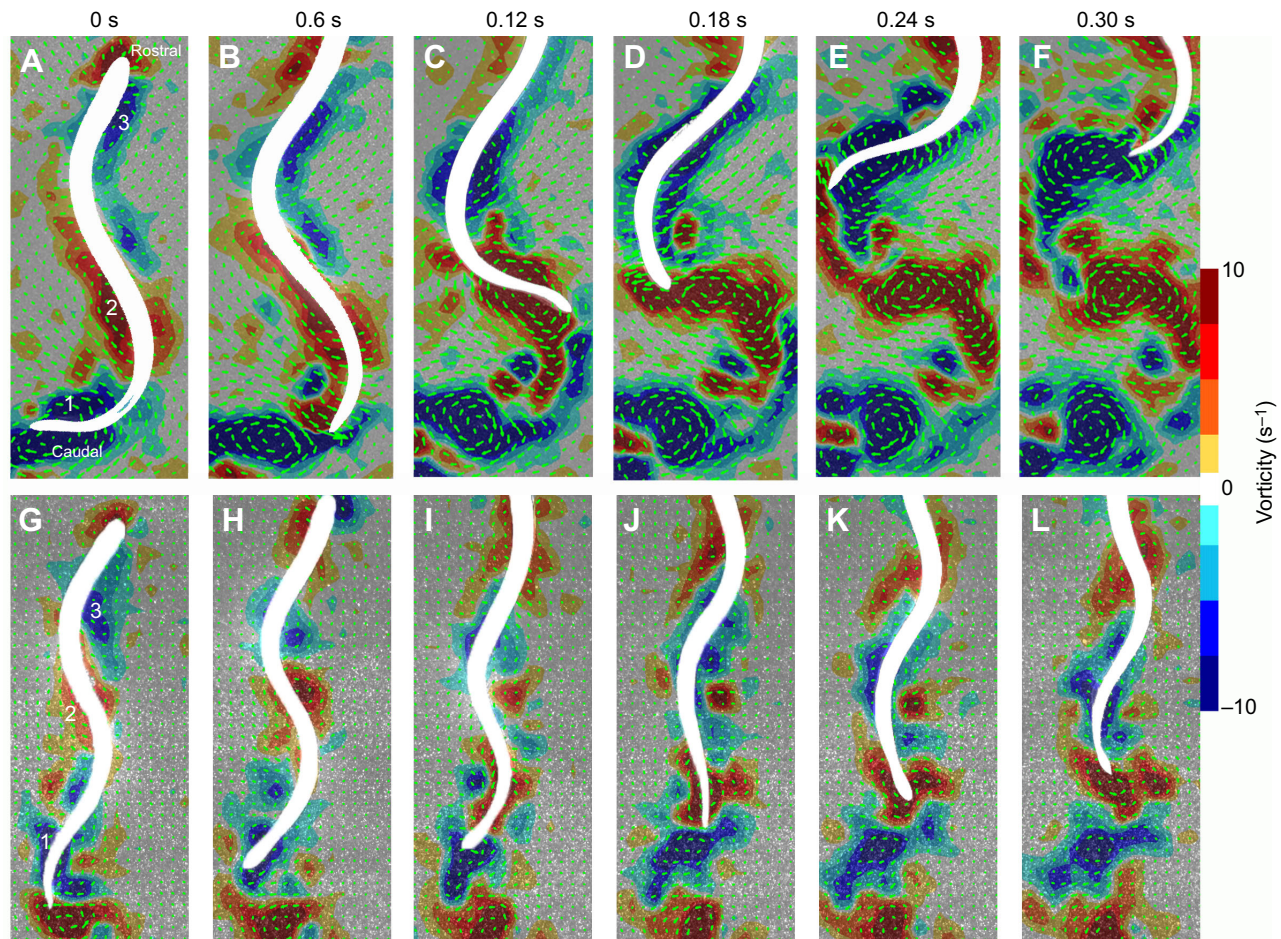
Fig. 3. Vorticity contours and velocity vectors around a swimming control and a mid-body transected lamprey over time. (A–F) Control; (G–L) mid-body transected. '1', '2' and '3' represent vortices 1–3 (see Figs 4 and 5).

Velocity fields collected via PIV were input to a custom program in MATLAB (Mathworks, Inc.) that computed the corresponding pressure fields. The algorithm integrates the Navier–Stokes equations along eight paths emanating from each point in the field of view, and it determines the pressure at each point by computing the median pressure from the eight integration results. The method has been previously validated against experimental and computational data, including numerical simulations of anguilliform swimming (Dabiri et al., 2014). The code is available to download for free at http://jodabiri.web.stanford.edu/largeweb/queen2.0.zip. The force contribution of each pressure component parallel to the direction of swimming (i.e. forward pull, rearward pull, forward push and rearward push) was determined by integrating each pressure component along the corresponding surfaces of the body. For the lamprey measurements, the force calculation was evaluated per unit depth, giving units of Newtons per centimeter of depth perpendicular to the measurement plane.

Statistical analysis

Statistical comparisons between the control and mid-body-transected lampreys involved Student's t-test comparisons between groups. All the data conformed to the assumptions of normality and homoscedasticity. The groups contained three control and two mid-body-transected lampreys. Fortunately, the very low levels of variability within groups enabled us to confidently detect difference between groups.

RESULTS
Comparison of body kinematics

In order to swim, the normal (control) lampreys used muscle actuation along the entire body (Williams et al., 1989) to generate a traveling wave that started at the head and traveled to the tail (Fig. 1A–C) and continually increased in amplitude along the length of the body (Fig. 1B,G). Only at the very tip of the tail did the amplitude decrease for the control lampreys. By contrast, the wave generated by the lampreys whose spinal cord was transected mid-body was a passive wave beyond the point of transection. It differed greatly from the control in that it had characteristics of a standing wave rather than a traveling wave (Fig. 1F), with a node-like location; however, it was not a true standing wave because the individual wave forms were not like that of a standing wave. In addition, the wave of the transected lampreys did not change in amplitude along the length of the body (Fig. 1E,G). Finally, the peak wavelength of the transected lampreys' body wave (0.59±0.18 body lengths) was smaller than the control lampreys (0.70±0.004 body lengths). The kinematics were highly consistent among the control lampreys but varied greatly among the transected individuals (e.g. the wavelength of the control only varied by 0.5%, whereas that of the transected varied by 30%). This perhaps is a result of the lack of body control by the transected lampreys below mid-body, leaving the tail to passively 'whip' around. The wavelength of the control lampreys remained constant. As a result of these body kinematics, the control lampreys swam nearly twice as fast as the transected
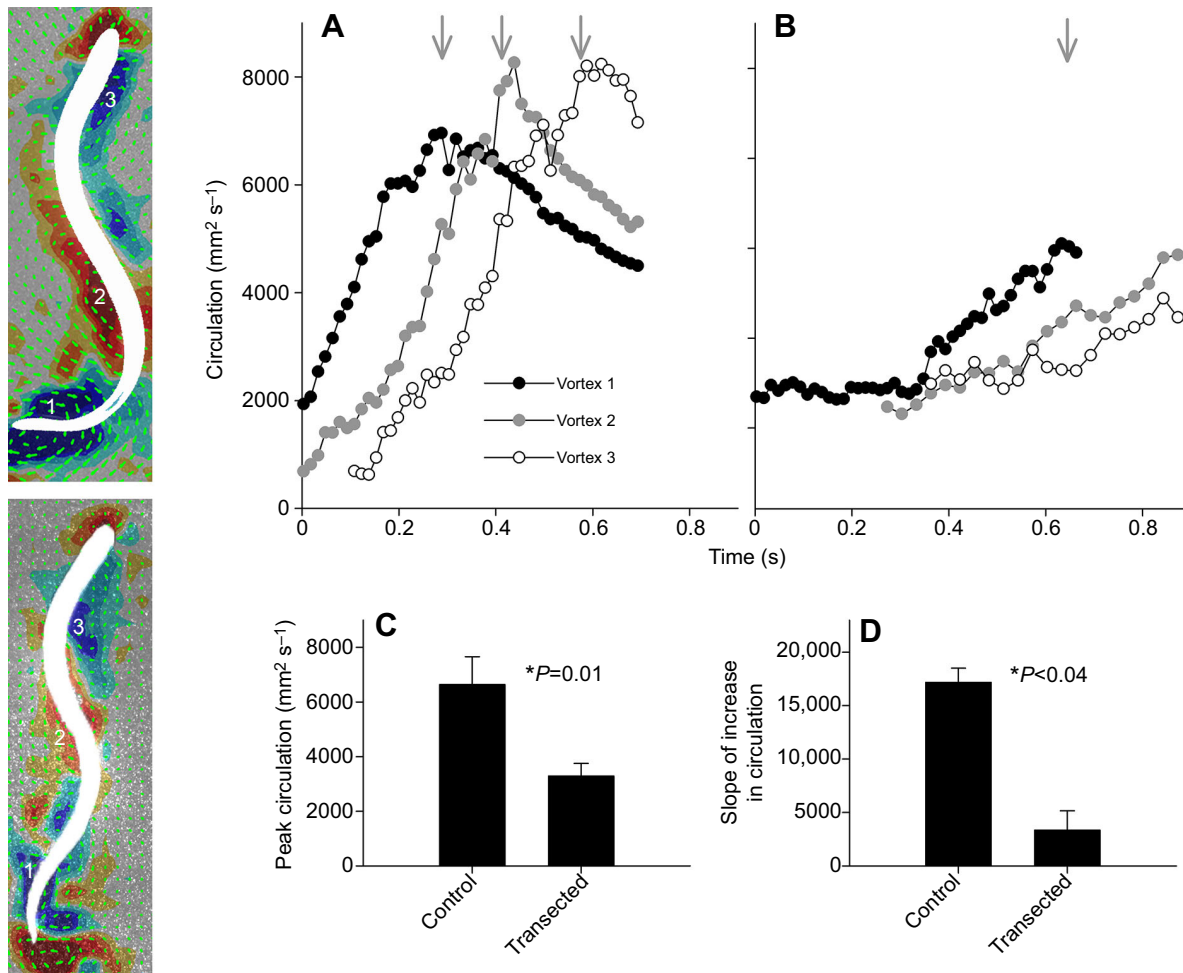
Fig. 4. Circulation of three successive vortices as they traveled along the body of the control and transected lampreys. Top contour image and A show the control, and the bottom image and B show a mid-body-transected lamprey. Arrows indicate when the vortices separated from the body. Notice that the vortices of the transected lamprey (B) are not shed and remain attached for a longer period of time. Comparison of the (C) means±s.d. peak circulation observed (Student's *t*-test, *N*=3 control and 2 mid-body transected) and the (D) means±s.d. slope that the circulation increased as it traveled from the head to the tail of the lampreys (Student's *t*-test, *N*=3 control and 2 mid-body transected).

lampreys (Fig. 1I; *t*-test; *P*<0.05). The ratio of the swimming speed and the wave speed (Fig. 1H) is the slip, which has been used by Lighthill (1969) and others to distinguish modes of fish kinematics. The control lampreys had a slightly higher slip, 0.74, than the transected lampreys, 0.65. Both were similar to other measured slips for eels (Gillis, 1996; Muller et al., 2001) and lampreys (Videler, 2012).

The body bending that generated the traveling wave caused the surface of the lamprey body to rotate. This rotation was measured as angular velocities associated with these bends. In fact, the bodies of both the control and transected lampreys had peak angular velocities around the peaks of the waves (Fig. 2A,B). The continually increasing amplitude of the body wave observed for the control lampreys (Fig. 1G) occurred because they were continually bending their body more as the wave propagated from head to tail. This caused the angular velocity of the control lampreys to continually increase as the wave traveled from head to tail (Fig. 2C). However, since the body amplitude of the transected lampreys did not increase, the angular velocities of the transected lampreys were highly variable and did not increase as the wave traveled from head to tail (Fig. 2C). This is because increased bending requires active actuation (Root et al., 2007), which the transected lampreys could

not do beyond mid-body. The amount of bending is important for vorticity generation. Its importance is seen in the direct and highly correlative relationship between the body surface angular velocity and the vorticity sign (Fig. 2D) and magnitude (Fig. 2E). This relationship was strong for both the control and transected lampreys.

Comparison of vorticity generation adjacent to the body

The influence of body kinematics on the hydrodynamic interactions ultimately determines swimming performance. Qualitatively, the PIV analysis illustrates how the body kinematics of the control lampreys accelerated the flow of the surrounding fluid much more than the kinematics of the transected lampreys, generating a much stronger vorticity field (Fig. 3). A comparison of the circulation confirms this (Fig. 4A,B), whereby the vorticity fields around the control lampreys had greater circulation levels (Fig. 4C; *t*-test; *P*=0.01). The control lampreys were able to generate these high circulation values because their body kinematics rapidly and continually increased circulation as the proto-vortices traveled along the body. Only after the vortices detached from the body, at the tail (indicated by the arrows in Fig. 4A,B), did the circulation decline. Body kinematics of transected lampreys generated

circulation, but they did not increase the circulation as well as the control lampreys did (Fig. 4D; *t*-test; *P*<0.04).

Comparison of vorticity control and interactions along the body

In addition to building vorticity, the kinematics of the control lampreys controlled the distance between the adjacent vortices (Fig. 5A). As a result, there was a separation between adjacent vortices at the tail of the control lampreys (Fig. 5C). The vortices along the bodies of the transected lampreys collided into each other as the vortices approached the tail (Fig. 5B) and, as a result, there was very little distance between adjacent vortices at the tail of these lampreys (Fig. 5C; *t*-test; *P*<0.02). Vorticity fields around the tail illustrate the separation and piling of vortices at the tail of control and transected lampreys, respectively (Fig. 6A,B).

The highest velocities along the lamprey body were located in the wave troughs at the interface between adjacent vortices (where the vortices converge). In this region, fluid flow was accelerated as the vortices travel along the body (Fig. 6C). Again, however, the fluid acceleration was much greater (i.e. slope of velocity build-up along the body) for the control lampreys (Fig. 6C,D). At the tail, where peak velocities were observed, the axial momentum flux of the control lampreys was an order of magnitude greater than in the transected animals (Fig. 6D). This was a result of: (a) greater fluid velocities adjacent to the control lampreys; (b) greater distances between the vortices; and (c) a greater proportion of the flow being directed axially (Fig. 6E).

Comparison of pressure fields and thrust generation

The intensifying vorticity and fluid velocities corresponded to pressure around the control lampreys becoming progressively more negative (Fig. 7A,C,D) as the body wave traveled posteriorly. Not

only did the negative pressure along the body intensify, but the size of the negative pressure region located in the trough of the body wave got progressively larger as the wave traveled toward the tail (Fig. 7D). However, for the transected lampreys, the minimum pressure did not decrease. In fact, the pressure along the body fluctuated considerably rather than trending more negative or positive (Fig. 7B,C,E).

The magnitude of the force in the axial direction, which contributed to forward thrust of the control lampreys, also intensified as the body wave traveled posteriorly (Fig. 8A,B,E). The thrust acting on the body bend was observed along the entire length of the control lampreys and it peaked just prior to the wave reaching the tail (Fig. 8A,B,E). This thrust was solely due to the negative pressure field located in the trough of the body wave. In fact, except for the small net thrust at the tail tip, the control lampreys were entirely pulled by negative pressure through the water. This contrasted sharply with the thrust that the transected lampreys generated (Fig. 8C,D,F). The transected lampreys generated most of their thrust near the tail and this was primarily due to positive high pressure pushing the tail forward (with a smaller contribution of negative pressure pulling the tail forward).

DISCUSSION
Effects of body kinematics on adjacent vorticity

Lampreys are a good model for examining hydrodynamic interactions along the body–fluid interface because their thrust is dominated by inertial rather than viscous forces and they build vorticity along their bodies gradually (Bale et al., 2014; Bhalla et al., 2013; Kern and Koumoutsakos, 2006; Muller et al., 2001). These properties enable us to quantify how the gradual development of important fluid interactions relate to thrust generation. The kinematics that we observed for our control lampreys have been commonly observed for other lampreys and anguilliform swimmers, where a traveling wave was initiated just posteriorly to the head and traveled toward the tail with continually increasing wave amplitude (Ayers et al., 1983; Chen et al., 2011; Davis et al., 1993; Lauder and Tytell, 2005). As the wave traveled, the adjacent fluid vorticity was aligned to characteristic sections of each bend as it traveled the length of the body, which has also been previously described (Muller et al., 2001; Videler et al., 1999; Wolfgang et al., 1999). With this alignment, the center of vorticity remained near the inflexion point of the bend and on the trough side of the body (Fig. 9C), and the adjacent vortices, rotating with opposite spin, converged at the wave trough (Fig. 9A). Our observations of how the vorticity along the body aligned with lamprey body bends were similar to what has been described for eels (Muller et al., 2001; Wolfgang et al., 1999). This is interesting because, in many of the eel studies, the eels were not in steady-state swimming (but were accelerating) and their kinematics had some differences from lampreys. Despite this, the influence of body bends on the adjacent hydrodynamics seems to remain similar. The formation of these body 'proto-vortices' have been attributed to a mechanism, termed undulatory pump, in which fluid is entrained and accelerated by positive (i.e. pushed) and negative (i.e. sucked) pressure regions that occur at the peak and trough of the wave, respectively (Fig. 9A; Blickhan et al., 1992; Müller et al., 1997; Videler et al., 1999). According to this mechanism, these pressure regions build vorticity and carry the vortices along the body with the traveling wave. However, although this mechanism plays a role in the flow along the body, another important mechanism is that the rotation of the body surface as it bends also rotates the adjacent fluid. This adds vorticity to the fluid (Fig. 9B) and controls how the fluid rotates relative to the
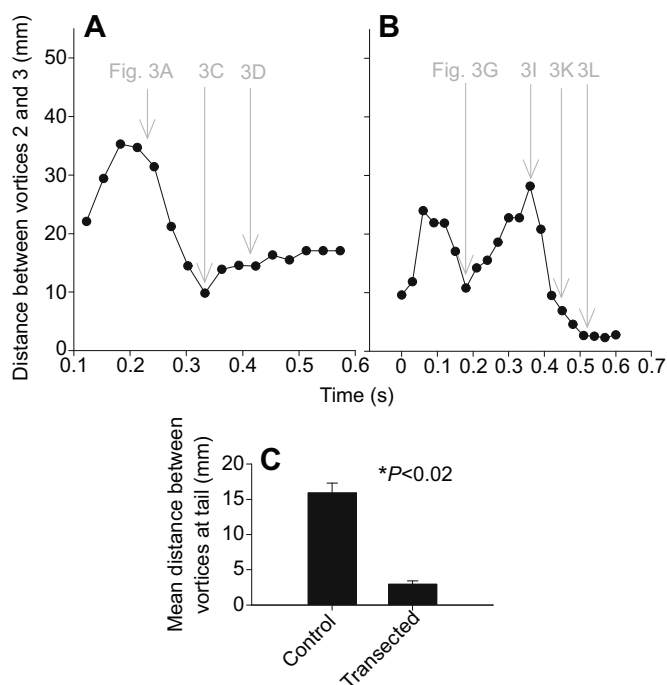

Fig. 5. Distance between adjacent vortices as they travel from the head to the tail of the control and the mid-body transected lampreys. (A) Control; (B) mid-body transected. (C) Means±s.d. distance between the vortices at the tail (Student's *t*-test, *N*=3 control and 2 mid-body transected). Distance was measured as the shortest distance between vorticity contours of 10 s^{-1}.
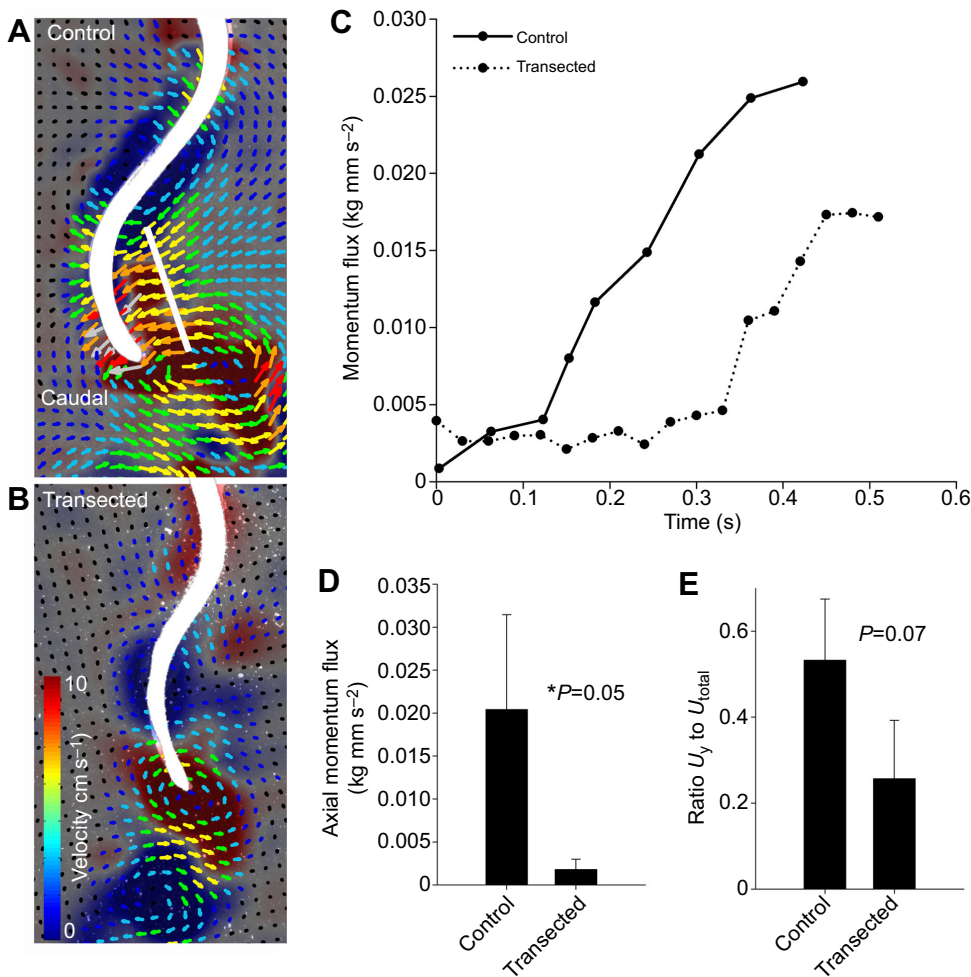
Fig. 6. Momentum flux of flow between adjacent vortices. Momentum fluxes were measured along transects joining adjacent vortices in the troughs of the body waves of the (A) control and (B) mid-body-transected lampreys. (C) Momentum flux as the vortices traveled from head to tail. (D) Means±s.d. axial momentum flux at the tail of the lamprey (Student's t-test, $N=3$ control and 2 mid-body transected) and (E) the means±s.d. ratio of the momentum flux in the axial direction (U_y) versus the total momentum flux (U_{total}) (Student's t-test, $N=3$ control and 2 mid-body transected).

body (Fig. 2). In fact, according to theory, vorticity of the fluid immediately adjacent to the body (no-slip fluid; White, 1991) should be twice the angular velocity of the body ($\Omega=2\omega$). Based on this, the angular velocity that we observed for the bending of control lampreys was sufficient to generate vorticity much greater than we observed in the surrounding fluid (PIV; Fig. 2F). This is consistent with our expectation to observe vorticity levels lower than predicted at a distance from the body surface. In addition, we saw for the control lampreys a continual increase in body bending as each body wave traveled toward the tail. This led to the increasing body amplitude and would serve to continually build fluid vorticity (Fig. 2F; Fig. 9D). In the transected lampreys, the amplitude did not continually increase, nor did the angular velocity of the body or the vorticity of the fluid. In addition to vorticity magnitude, the direction of body bending, for both the control and transected lampreys, correlated very closely with the direction of the fluid vorticity (Fig. 2C–E). Therefore, using both pressure (i.e. undulatory pump) and viscous (i.e. body surface rotation) mechanisms, flexible bending of the body controls the alignment and builds the magnitude of adjacent vortices (Fig. 9C).

The importance of active bending for vorticity control was evident in how effectively the control lampreys maintained spacing between adjacent vortices as the vortices travel toward the tail. In contrast, the vortices of the transected lampreys, whose bending kinematics past mid-body was completely passive, collided in the tail region. The convergence of the vortices of the transected lampreys at the tail coincided with a decrease in the wavelength of

the body waves, suggesting that the distance between the vortices on each side of the wave trough is at least partially controlled by body wavelength. Active muscle contractions stiffen the body, which increases the wavelength of the bending waves (Williams et al., 1989). Additionally, the control lampreys were able to avoid the build-up of vortices at the tail by actively sweeping the tail in the opposite direction, shedding the trailing vortex before the adjacent vortex approached. Computational studies of lamprey swimming confirm the need for active suppression of passive kinematics for improved propulsion (Root et al., 2007). Since vortices align along the same part of the body bend, active control of bending is necessary to control the wave shape and therefore vortex interactions.

Hydrodynamic effects of interactions between adjacent vortices

In the control lampreys, the traveling bends built vorticity and moved vortices toward the tail region, where vorticity levels peaked. In addition to vorticity, the fluid velocity in the wave trough increased as the wave traveled along the body (Fig. 6A). In the trough of the wave at the tail, we observed the maximum velocities in the fluid around the control lampreys. This 'jet' has been previously identified as the primary thrust signature for undulatory swimmers (Leftwich, 2010; Tytell and Lauder, 2004; Videler et al., 1999); however, the role of vortices in generating this 'jet' has not been well described. Although the undulatory pump mechanism has been used to describe the jet formation (Videler et al., 1999), we
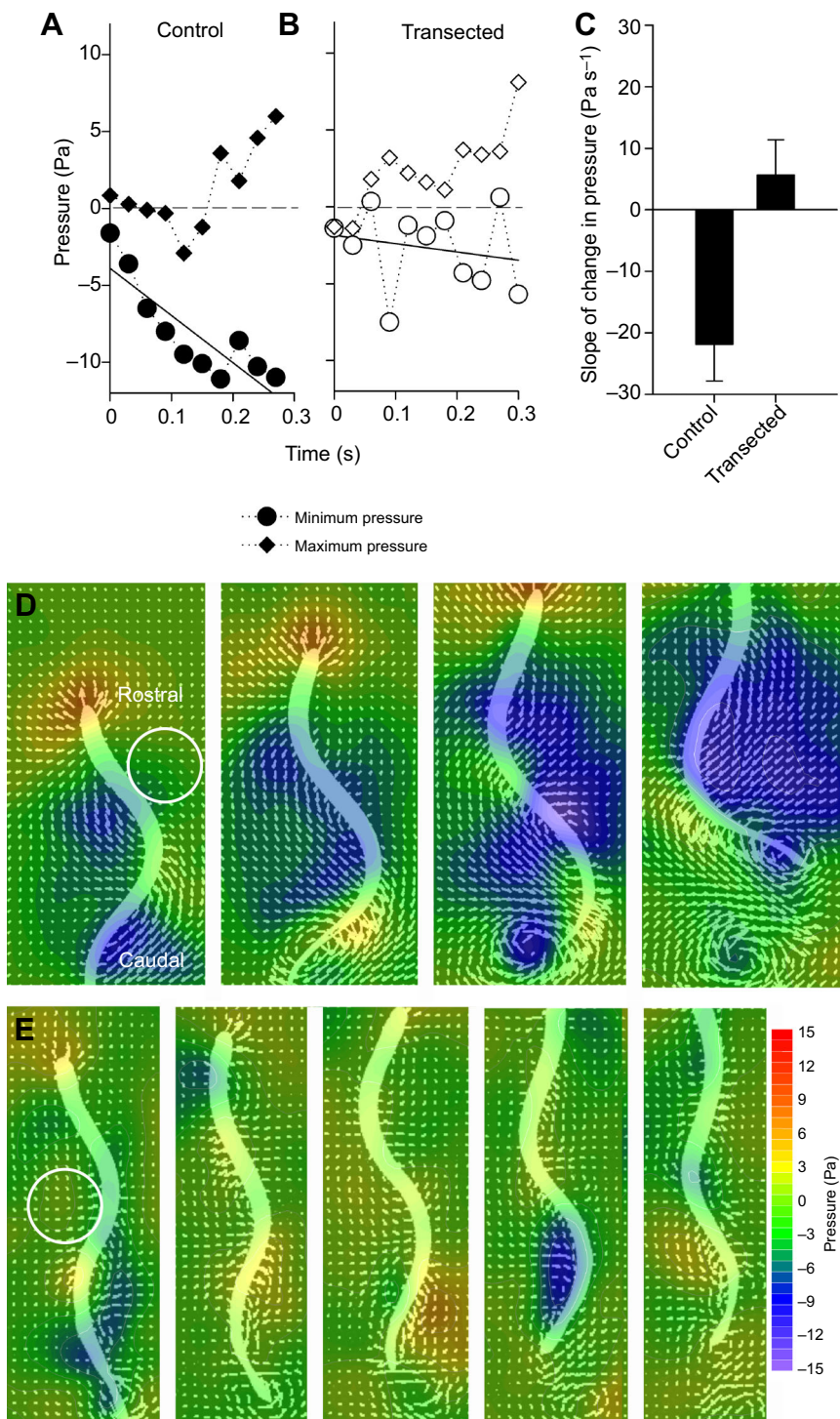
Fig. 7. Change in the pressure field around the body wave as it travels from head to tail in control and transected lamprey. The minimum pressure was measured on the anterior-facing side of the wave (trough; indicated by circle in D and E). The maximum was measured on the posterior side (hump of wave). (C) The means±s.d. of the slope of the change in the minimum pressure among control (*n*=2) and transected (*n*=2) lampreys. Sequential images of the (D) control and (E) transected lampreys with 0.06 s intervals between images.

found and others have shown (Muller et al., 2001) that most of the flow along the body is contained in the proto-vortices until they reach the tail. Furthermore, the jet is straight with little vorticity and is located in the region where two adjacent, oppositely spinning, proto-vortices interact. Elevated velocities and momentum fluxes have been demonstrated to be generated (both numerically and experimentally) at the interface between two converging vortices with opposite spin. In this region, angular components of the fluid cancel out and the flow of the water is greatly accelerated (Stanaway et al., 1988). Thus, we observe this as a straight jet (Fig. 9E).

Recently, it has been shown that these interactions at the interface of vortices can enhance thrust (Fu and Liu, 2015). However, this effect is highly dependent on vortex spacing (Fu and Liu, 2015) and is controlled by the local vorticity conditions (Stanaway et al., 1988). We argue that, by maintaining a constant distance between adjacent vortices, the bending kinematics of the control lampreys controlled the interaction of the adjacent vortices, whose circulation grew as they traveled toward the tail but whose spacing was kept constant. The confluence of these conditions served to increase the interaction of the vortices in a controlled manner that accelerated the fluid flow
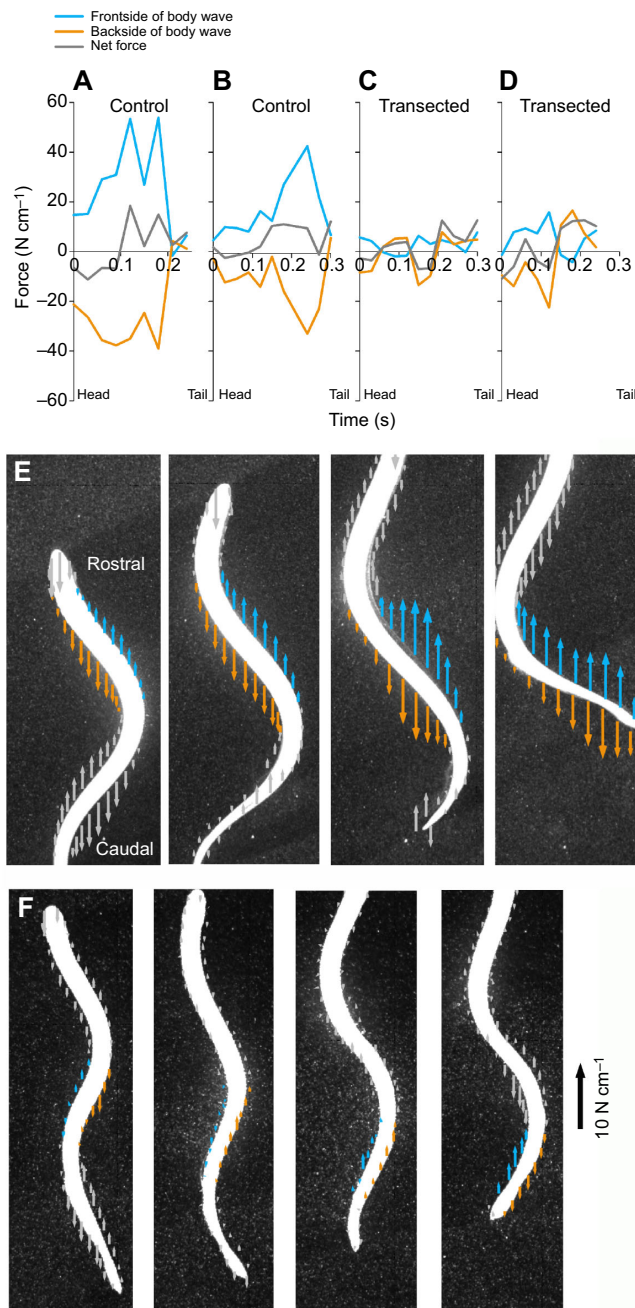
Fig. 9. Schematic describing mechanisms by which body kinematics build and control body vortices. (A) Undulatory pump mechanism whereby body waves entrain surrounding fluid using low-pressure regions [suction (S)] in the wave troughs, which move fluid toward the body, and high-pressure regions [push (P)] along the wave peaks, which move fluid away. (B) Body surface rotation mechanism whereby the surface of the body has rotation as it bends, which rotates the fluid (vorticity of no-slip fluid=2×angular velocity of body surface). (C) Combined, these two mechanisms build vortices, which align along specific parts of the traveling wave. Diamond indicates position of inflexion point of the body bend. Blue and red ovals show where oppositely spinning vortices align along the body (rotation within each vortex ring are indicated by green arrows). (D) The increased bending of the body that occurs as the wave travels from the head to the tail builds vorticity and, at the interface of oppositely rotating vortices, fluid flow is accelerated (indicated by arrows). (E) Close-up of interactions at a vortex interface, which accelerate fluid flow. (F) The vortices and the accelerated fluid flow are hydrodynamic features that create negative pressures in the fluid. These features along the lamprey body result in large negative pressure regions in the wave troughs.

Fig. 8. Force magnitude along the posterior half of the traveling body wave as the wave travels from head to tail in the control and transected individuals. (A–D) Each graph shows replicate individuals, $n=2$. The net force (gray line) is the sum of the axially (blue line, and blue vectors in E and F) and posteriorly (orange line, and orange vectors in E and F) facing surfaces of the wave. Positive or negative values correspond to thrust or drag forces, respectively. Positive blue lines (and vectors in E and F) are pulling forces (due to negative pressure) and positive orange lines (and vectors in E and F) are pushing forces (due to positive pressure). (E,F) Sequential images with force vectors (0.06 s interval between images). The gray vectors were not considered for the time series (A–D) but show the forces along the whole body and demonstrate that the patterns seen in the colored quantified region are repeated on each side of the body and with each body wave.

Pressure and thrust resulting from different hydrodynamic conditions

How do these different hydrodynamic conditions explain the differences in thrust? We and others (Bale et al., 2014; Bhalla et al., 2013; Kern and Koumoutsakos, 2006; Muller et al., 2001; Videler et al., 1999; Wolfgang et al., 1999) have shown that the bending kinematics build and align vortices around the troughs of the traveling waves. We have shown that active control of bending is crucial for lampreys to enhance these hydrodynamic features (i.e. high circulation and 'jets'). Both vortices and accelerated velocities are hydrodynamic features associated with and directly related to zones of negative pressure in the fluid (Batchelor, 1973; Li et al., 2012), and, for the control lampreys, the gradual development of these hydrodynamic features gradually developed large negative pressure zones in the troughs of the traveling waves (Fig. 9F; Gemmell et al., 2015). It was the pull from these negative pressure

and built momentum flux at the vortex interface. For the transected lampreys, neither of these conditions was observed: the vorticity did not grow and the vortices collided in the tail region, which prevented the large build-up of momentum at the tail.
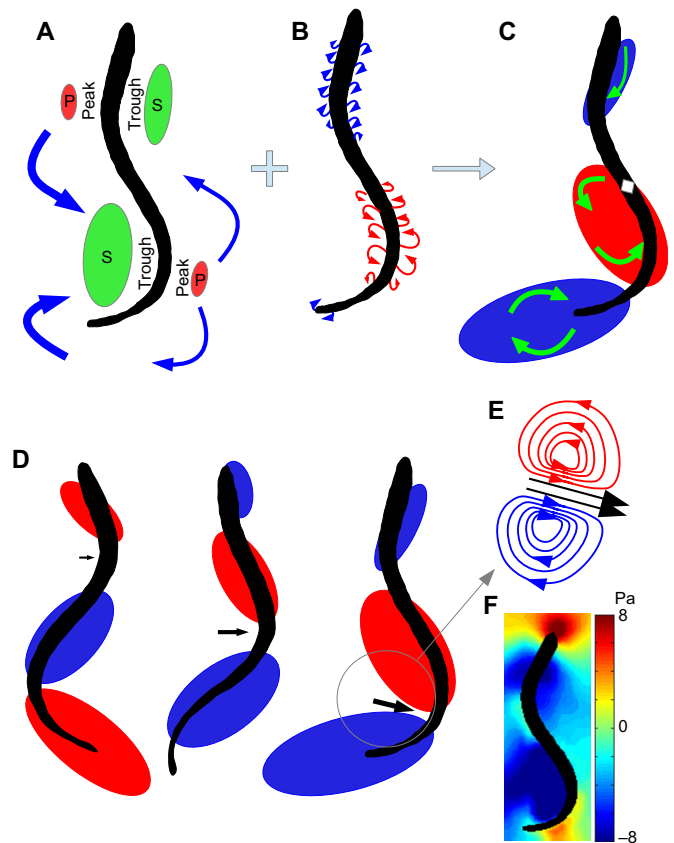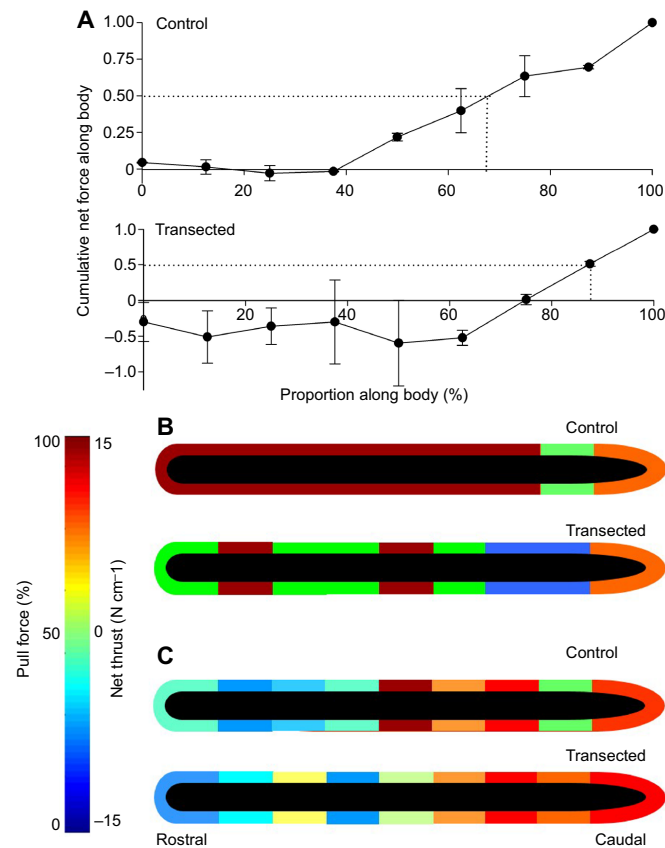
Fig. 10. Thrust forces along the lamprey body. (A) Cumulative net force of the control (*n*=2) and transected (*n*=2) lampreys along the body. (B) Schematic of the percent of the thrust (mean, *n*=2 control and *n*=2 transected) from negative pressure pulling, showing that the force acting on the control lampreys is almost exclusively pulling, whereas the transected animals is mostly pushing [especially when the net force acting on the lamprey is forward (C)]. (C) Net force (mean, *n*=2 control and *n*=2 transected) acting on different portions of the lamprey body showing that, for the control, a lot of the positive thrust occurs anteriorly to the tail, whereas it is positive at the tail of the transected lamprey.

regions on the anteriorly oriented parts of the body along the wave troughs that was the primary thrust mechanism pulling the control lampreys forward (Fig. 10B). This suction thrust grew as the wave traveled down the body; as a result, the control lampreys received the bulk of their total thrust (~75%) along their body anteriorly to their tail (Fig. 10A). In contrast, propulsion without the build-up of these hydrodynamic features, as is seen in the transected lampreys, relied largely on positive pressure fields pushing on the lamprey tails (Fig. 10B). These fields are smaller and not as extreme as the negative pressure fields seen around the control lamprey; therefore, the magnitude of thrust is much smaller. Negative pressure zones have been known to contribute to thrust (Bale et al., 2014; Li et al., 2012; Liu et al., 1996); however, the importance of forces pulling swimming animals forward has not been realized. The realization that anguilliform lampreys rely on negative pressure zones for thrust elevates the importance of bending kinematics because of how directly these forces generate and control vorticity to always form negative pressure fields.

It is important to distinguish the negative pressure fields and corresponding axially directed suction thrust used by lampreys from the negative pressure fields that many animals are known to create in the process of generating lift forces for swimming. Lift forces are by definition oriented perpendicular to the direction of body motion, and are the result of 'bound vorticity' in the wing or fin (Vogel,

2013). By contrast, the negative pressure fields exploited by the lampreys form due to vortices external to the body and due to accelerated flow at the interface of adjacent vortices.

Relation to other types of fish propulsion

Without direct analysis it is difficult to say how important the mechanisms of body bending described for lampreys are for other swimming animals. However, there is remarkable similarity in the bending kinematics of both swimming and flying animals (Lucas et al., 2014), suggesting that the role of bending may also be similar among swimming and flying animals. We described two mechanisms by which bending forms and aligns vorticity, one pressure based (Fig. 9A) the other viscous based (Fig. 9B). As mentioned, the kinematics of anguilliform lampreys builds vorticity in the fluid gradually. The gradual build-up of vorticity probably enables the body surface rotation to have a stronger influence on the fluid, increasing the role of this mechanism in thrust production in lampreys and other anguilliform swimmers. It also results in a gradual build-up of pressure gradients in the fluid (Fig. 7; Gemmell et al., 2015), reducing the muscle power required for anguilliform swimming compared to other types of fish propulsion, i.e. carangiform and tunniform. This may explain the low cost of transport observed among anguilliform swimmers (van den Thillart et al., 2007). However, the observed increasing amplitude of the bending body toward the tail is directly related to the body surface rotation and is a ubiquitous trait of swimming fish, regardless of the type of fish. This strongly suggests that most fish rely on body surface rotation to build and control vortices. Another interesting observation is that animals that are able to crawl on land and swim in the water use completely different body wave kinematics between terrestrial and aquatic propulsion (Gillis, 1998; Graham et al., 1987; Maladen et al., 2009). While crawling on land, the body waves of eels and snakes do not change their amplitude from head to tail; however, when swimming in water they do increase their body amplitude, which leads to increased body surface rotation. Therefore, the need to bend more in water than when on land suggests that body surface rotation is an important kinematic feature necessary for generating swimming thrust.

Another important feature of the body bending described for lamprey, and which has been shown for fish larvae (Li et al., 2012), is that the negative pressure regions primarily developed along the concave portions of the body bends. We can look at the midline kinematics of other fish propulsive modes to see whether their body waves also develop these concave regions to speculate on the importance of negative pressure fields in generating thrust for these other modes. The amount of concavity seems to decrease moving along the propulsive gradient from anguilliform to carangiform to tunniform swimmers (Lauder and Tytell, 2005). Based on this, we would speculate that the importance of negative pressure fields for thrust also decreases along this gradient. Interestingly, fish that use these other swimming modes, such as tuna and salmon, have a higher cost of transportation than eels and lamprey (William and Beamish, 1979; Sepulveda and Dickson, 2000; Lee et al., 2003; van Ginneken et al., 2005). This may be in part be because their swimming modes, although good for proficiency, do not have the energetic benefits associated with suction thrust (Gemmell et al., 2015). However, these are only hypotheses; without quantification of the pressure fields around other swimmers it is difficult to speculate about the role of negative versus positive pressure in generating thrust.

Conclusion

Our study confirms the current knowledge of how effectively traveling body waves, which bend the lamprey body, generate and

control vortices, but also expands our understanding of the importance of active kinematics and increasing wave amplitude for the ability to grow vortices and fluid velocities. In addition, we show that the gradual growth of these hydrodynamic features directly relate to the growth of negative pressure fields, which are the primary thrust mechanism and which serve to pull non-transected lampreys through the water. Non-optimal, passive kinematics can generate thrust but it seems to have a completely different hydrodynamic basis, which results in positive pressures dominating thrust at the tail. We are just beginning to fully appreciate the role of bending for propulsion and more work may soon enable engineers to incorporate controlled bending kinematics to improve the efficiency and maneuverability of engineered vehicles.

Supplementary information
Supplementary information available online at
http://jeb.biologists.org/lookup/doi/10.1242/jeb.144642.supplemental

References
Alben, S. (2008). Optimal flexibility of a flapping appendage in an inviscid fluid. *J. Fluid Mech.* **614**, 355-380.

Ayers, J., Carpenter, G. A., Currie, S. and Kinch, J. (1983). Which behavior does the lamprey central motor program mediate? *Science* **221**, 1312-1314.

Bale, R., Shirgaonkar, A. A., Neveln, I. D., Bhalla, A. P. S., MacIver, M. A. and Patankar, N. A. (2014). Separability of drag and thrust in undulatory animals and machines. *Sci. Rep.* **4**, 7329.

Bale, R., Neveln, I. D., Bhalla, A. P. S., MacIver, M. A. and Patankar, N. A. (2015). Convergent evolution of mechanically optimal locomotion in aquatic invertebrates and vertebrates. *PLoS Biol.* **13.4**, e1002123.

Bandyopadhyay, P. R. (2005). Trends in biorobotic autonomous undersea vehicles. *IEEE J. Oceanic Eng.* **30**, 109-139.

Bartol, I. K., Krueger, P. S., Stewart, W. J. and Thompson, J. T. (2009). Hydrodynamics of pulsed jetting in juvenile and adult brief squid *Lolliguncula brevis*: evidence of multiple jet 'modes' and their implications for propulsive efficiency. *J. Exp. Biol.* **212**, 1889-1903.

Batchelor, G. K. (1973). *An Introduction to Fluid Mechanics*. Cambridge, UK: Cambridge University Press.

Bhalla, A. P. S., Griffith, B. E. and Patankar, N. A. (2013). A forced damped oscillation framework for undulatory swimming provides new insights into how propulsion arises in active and passive swimming. *PLoS Comput. Biol.* **9**, e1002123.

Blickhan, R., Krick, C., Zehren, D., Nachtigall, W. and Breithaupt, T. (1992). Generation of a vortex chain in the wake of a Suhundulatory swimmer. *Naturwissenschaften* **79**, 220-221.

Chen, J., Friesen, W. O. and Iwasaki, T. (2011). Mechanisms underlying rhythmic locomotion: body–fluid interaction in undulatory swimming. *J. Exp. Biol.* **214**, 561-574.

Colin, S. P., Costello, J. H., Dabiri, J. O., Villanueva, A., Blottman, J. B., Gemmell, B. J. and Priya, S. (2012). Biomimetic and live medusae reveal the mechanistic advantages of a flexible bell margin. *PLoS ONE* **7.11**, e48909.

Dabiri, J. O., Colin, S. P., Katija, K. and Costello, J. H. (2010). A wake-based correlate of swimming performance and foraging behavior in seven co-occurring jellyfish species. *J. Exp. Biol.* **213**, 1217-1225.

Dabiri, J. O., Bose, S., Gemmell, B. J., Colin, S. P. and Costello, J. H. (2014). An algorithm to estimate unsteady and quasi-steady pressure fields from velocity field measurements. *J. Exp. Biol.* **217**, 331-336.

Davis, G. R., Jr, Troxel, M. T., Kohler, V. J., Grossmann, E. M. and McClellan, A. D. (1993). Time course of locomotor recovery and functional regeneration in spinal-transected lamprey: kinematics and electromyography. *Exp. Brain Res.* **97**, 83-95.

Dickinson, M. H., Farley, C. T., Full, R. J., Koehl, M. A. R., Kram, R. and Lehman, S. (2000). How animals move: an integrative view. *Science* **288**, 100-106.

Fu, Z. and Liu, H. (2015). Transient force augmentation due to counter-rotating vortex ring pairs. *J. Fluid Mech.* **785**, 324-348.

Gemmell, B. J., Costello, J. H., Colin, S. P., Stewart, C. J., Dabiri, J. O., Tafti, D. and Priya, S. (2013). Passive energy recapture in jellyfish contributes to propulsive advantage over other metazoans. *Proc. Natl. Acad. Sci. USA* **110**, 17904-17909.

Gemmell, B. J., Colin, S. P., Costello, J. H. and Dabiri, J. O. (2015). Suction-based propulsion as a basis for efficient animal swimming. *Nat. Commun.* **6**, 8790.

Gillis, G. B. (1996). Undulatory locomotion in elongate aquatic vertebrates: anguilliform swimming since Sir James Gray. *Am. Zool.* **36**, 656-665.

Gillis, G. B. (1998). Environmental effects on undulatory locomotion in the American eel *Anguilla rostrata*: kinematics in water and on land. *J. Exp. Biol.* **201**, 949-961.

Graham, J. B., Lowell, W. R., Rubinoff, I. and Motta, J. (1987). Surface and subsurface swimming of the sea snake *Pelamis platurus*. *J. Exp. Biol.* **127**, 27-44.

Jacobs, A. J., Swain, G. P., Snedeker, J. A., Pijak, D. S., Gladstone, L. J. and Selzer, M. E. (1997). Recovery of neurofilament expression selectively in regenerating reticulospinal neurons. *J. Neurosci.* **17**, 5206-5220.

Kern, S. and Koumoutsakos, P. (2006). Simulations of optimized anguilliform swimming. *J. Exp. Biol.* **209**, 4841-4857.

Krueger, P. S. and Gharib, M. (2003). The significance of vortex ring formation to the impulse and thrust of a starting jet. *Phys. Fluids* **15**, 1271-1281.

Lauder, G. V. and Tytell, E. D. (2005). Hydrodynamics of undulatory propulsion. *Fish Physiol.* **23**, 425-468.

Lee, C. G., Farrell, A. P., Lotto, A., MacNutt, M. J., Hinch, S. G. and Healey, M. C. (2003). The effect of temperature on swimming performance and oxygen consumption in adult sockeye (*Oncorhynchus nerka*) and coho (*O. kisutch*) salmon stocks. *J. Exp. Biol.* **206**, 3239-3251.

Leftwich, M. C. (2010). *The Hydrodynamics of Lamprey Locomotion*. Princeton, NJ: Princeton University.

Li, G., Müller, U. K., van Leeuwen, J. L. and Liu, H. (2012). Body dynamics and hydrodynamics of swimming fish larvae: a computational study. *J. Exp. Biol.* **215**, 4015-4033.

Lighthill, M. J. (1969). Hydromechanics of aquatic animal propulsion. *Annu. Rev. Fluid Mech.* **1**, 413-446.

Linden, P. F. and Turner, J. S. (2004). 'Optimal' vortex rings and aquatic propulsion mechanisms. *Proc. R. Soc. B Biol. Sci.* **271**, 647-653.

Liu, H., Wassersug, R. and Kawachi, K. (1996). A computational fluid dynamics study of tadpole swimming. *J. Exp. Biol.* **199**, 1245-1260.

Lucas, K. N., Johnson, N., Beaulieu, W. T., Cathcart, E., Tirrell, G., Colin, S. P., Gemmell, B. J., Dabiri, J. O. and Costello, J. H. (2014). Bending rules for animal propulsion. *Nat. Commun.* **5**, 3293.

Lucas, K. N., Thornycroft, P. J. M., Gemmell, B. J., Colin, S. P., Costello, J. H. and Lauder, G. V. (2015). Effects of non-uniform stiffness on the swimming performance of a passively-flexing, fish-like foil model. *Bioinspir. Biomim.* **10**, 056019.

Maladen, R. D., Ding, Y., Li, C. and Goldman, D. I. (2009). Undulatory swimming in sand: subsurface locomotion of the sandfish lizard. *Science* **325**, 314-318.

Mountcastle, A. M. and Daniel, T. L. (2010). Vortexlet models of flapping flexible wings show tuning for force production and control. *Bioinspir. Biomim.* **5**, 045005.

Müller, U., Van Den Heuvel, B., Stamhuis, E. and Videler, J. (1997). Fish foot prints: morphology and energetics of the wake behind a continuously swimming mullet (*Chelon labrosus* Risso). *J. Exp. Biol.* **200**, 2893-2906.

Muller, U. K., Smit, J., Stamhuis, E. J. and Videler, J. J. (2001). How the body contributes to the wake in undulatory fish swimming: flow fields of a swimming eel (*Anguilla anguilla*). *J. Exp. Biol.* **204**, 2751-2762.

Nakata, T. and Liu, H. (2012). Aerodynamic performance of a hovering hawkmoth with flexible wings: a computational approach. *Proc. R. Soc. Lond. B Biol. Sci.* **279**, 722-731.

Nauen, J. C. and Lauder, G. V. (2002). Hydrodynamics of caudal fin locomotion by chub mackerel, *Scomber japonicus* (Scombridae). *J. Exp. Biol.* **205**, 1709-1724.

Oliphint, P. A., Alieva, N., Foldes, A. E., Tytell, E. D., Lau, B. Y. B., Pariseau, J. S., Cohen, A. H. and Morgan, J. R. (2010). Regenerated synapses in lamprey spinal cord are sparse and small even after functional recovery from injury. *J. Comp. Neurol.* **518**, 2854-2872.

Root, R. G., Courtland, H.-W., Shepherd, W. and Long, J. H., Jr (2007). Flapping flexible fish. *Exp. Fluids* **43**, 779-797.

Sepulveda, C. and Dickson, K. A. (2000). Maximum sustainable speeds and cost of swimming in juvenile kawakawa tuna (*Euthynnus affinis*) and chub mackerel (*Scomber japonicus*). *J. Exp. Biol.* **203**, 3089-3101.

Stanaway, S., Shariff, K. and Hussain, F. (1988). Head-on collision of viscous vortex rings. In *Proceedings of the Summer Program*, pp. 287-309. Stanford, CA: Stanford University Press.

Tytell, E. D. (2004). The hydrodynamics of eel swimming II. Effect of swimming speed. *J. Exp. Biol.* **207**, 3265-3279.

Tytell, E. D. and Lauder, G. V. (2004). The hydrodynamics of eel swimming I. Wake structure. *J. Exp. Biol.* **207**, 1825-1841.

Tytell, E. D., Hsu, C.-Y., Williams, T. L., Cohen, A. H. and Fauci, L. J. (2010). Interactions between internal forces, body stiffness, and fluid environment in a neuromechanical model of lamprey swimming. *Proc. Natl. Acad. Sci. USA* **107**, 19832-19837.

van den Thillart, G., Palstra, A. and Van Ginneken, V. (2007). Simulated migration of European silver eel; swim capacity and cost of transport. *J. Mar. Sci. Technol.* **15**, 1-16.

van Ginneken, V., Antonissen, E., Müller, U. K., Booms, R., Eding, E., Verreth, J. and van den Thillart, G. (2005). Eel migration to the Sargasso: remarkably high swimming efficiency and low energy costs. *J. Exp. Biol.* **208**, 1329-1335.

Videler, J. J. (2012). *Fish Swimming*. London: Chapman and Hall.

Videler, J., Muller, U. and Stamhuis, E. (1999). Aquatic vertebrate locomotion: wakes from body waves. *J. Exp. Biol.* **202**, 3423-3430.

Vogel, S. (2013). *Comparative Biomechanics: Life's Physical World*. Princeton, NJ: Princeton University Press.

White, F. (1991). *Viscous Fluid Flow, 1991*, pp. 335-393. New York: MacGraw.

William, F. and Beamish, H. (1979). Migration and spawning energetics of the anadromous sea lamprey, *Petromyzon marinus*. *Environ. Biol. Fish.* **4**, 3-7.

Williams, T. L., Grillner, S., Smoljaninov, V. V., Allen, P. W., Kashin, S. and Rossignol, S. (1989). Short communication locomotion in lamprey and trout: the relative timing of activation and movement. *J. Exp. Biol* **143**, 559-566.

Wolfgang, M. J., Anderson, J. M., Grosenbaugh, M. A., Yue, D. K. and Triantafyllou, M. S. (1999). Near-body flow dynamics in swimming fish. *J. Exp. Biol.* **202**, 2303-2327.

Zhang, G., Jin, L.-Q., Sul, J.-Y., Haydon, P. G. and Selzer, M. E. (2005). Live imaging of regenerating lamprey spinal axons. *Neurorehabil. Neural Repair* **19**, 46-57.
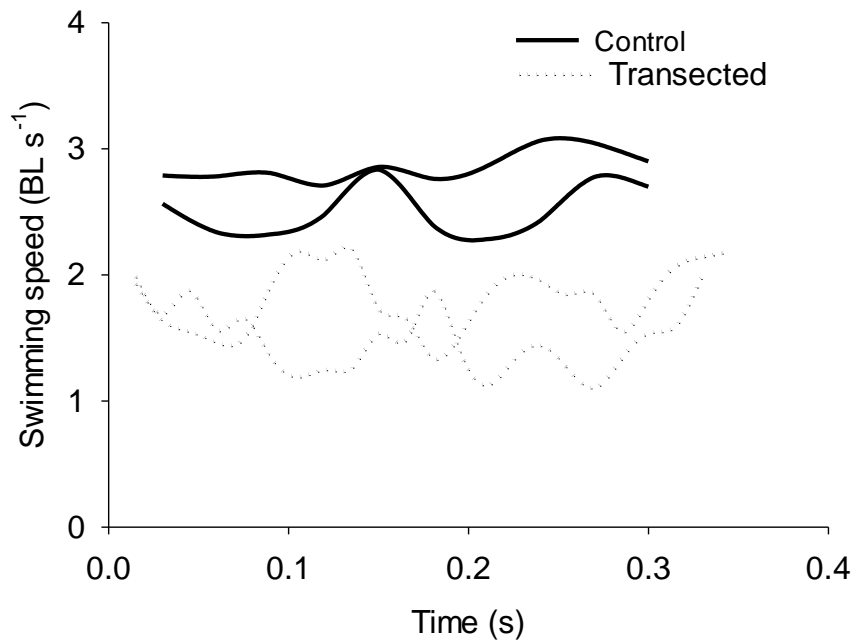
Figure S1. Instantaneous swimming velocity (normalized by body length) of the control (solid lines) and transected (dotted lines) lampreys. Each line is a different individual. While the instantaneous velocity of the lampreys changed constantly, the velocity averaged over each swimming cycle remained constant.